BIOCHEMISTRY
including biophysical chemistry & molecular biology

Article

pubs.acs.org/biochemistry

Proton Association Constants of His 37 in the Influenza-A $M2_{18-60}$ Dimer-of-Dimers

Michael T. Colvin,[†] Loren B. Andreas,[†] James J. Chou,[‡] and Robert G. Griffin*,[†]

[†]Department of Chemistry and Francis Bitter Magnet Laboratory, Massachusetts Institute of Technology, Cambridge, Massachusetts 02139, United States

[‡]Department of Biological Chemistry and Molecular Pharmacology, Harvard Medical School, Boston, Massachusetts 02115, United States

Supporting Information

ABSTRACT: The membrane protein M2 from influenza-A forms a single-pass transmembrane helix that assembles in lipid membrane as homotetramers whose primary function is to act as a proton transporter for viral acidification. A single residue, histidine 37 (His 37), is known to be responsible for selectivity and plays an integral role in the protein's function. We report pH-dependent ^{15}N MAS NMR spectra of His 37 within the influenza-A proton conduction domain of M2, $M2_{18-60}$, which has been previously shown to be a fully functional construct and was recently determined to adopt a dimer-of-dimers structure in lipids. By extracting the ratio of [His]/[HisH$^+$] as a function of pH, we obtained two doubly degenerate proton disassociation constants, 7.63 ± 0.15 and 4.52 ± 0.15, despite a possible maximum of four. We also report the $^1H_{N\varepsilon}$ chemical shifts at pH 6.5 recorded at 60 kHz MAS in a CP-based $^1H-^{15}N$ spectrum. We were unable to detect resonances indicative of direct proton sharing among His 37 side chains when the tetramer is in the +2 state. In the neutral state, His 37 is exclusively in the τ tautomer, indicating that the δ nitrogen is protonated solely as a function of pH. We also found that the plot of [HisH$^+$]/[His] as a function of pH is qualitatively similar to previously reported proton conduction rates, indicating that proton conduction rate is proportional to the level of histidine protonation within the channel. Two-dimensional $^{13}C-^{13}C$ and $^{13}C-^{15}N$ correlations suggest that at low pH multiple conformations are populated as the spectra broaden and eventually disappear as the acidity is increased. A second highly resolved state at low pH was not observed.

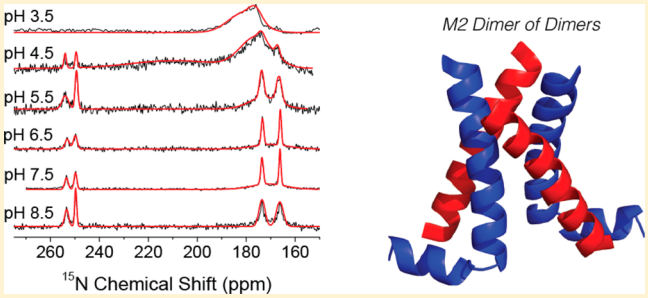

The M2 protein of influenza-A is a 97 amino acid protein with one transmembrane domain that forms homotetramers whose primary function is to conduct protons across the viral membrane. At the pH of the cytosol, M2 is inefficient for conducting protons. However, the low pH of the host cells' endosome activates M2 and acidifies the viral interior by conducting protons with near perfect selectivity.[1] Although the rate is relatively slow (10^1-10^4 s^{-1}),[2] it allows for unpacking of viral ribonucleoprotein into the host cell.[1,3] M2 may also play a role in maintaining the high pH of the trans-Golgi network.[1] A single residue, histidine 37 (His 37), located in the transmembrane region is known to be responsible for pH activation and selectivity, whereas a second residue, tryptophan 41 (Trp 41), is responsible for unidirectional proton conduction and is found one helical turn below His 37, both of which are universally conserved in a variety of functional mutants.[1,4] M2 has been the subject of investigation since it was discovered to be the target of adamantyl amine based inhibitors, and the functional binding site for these drugs was subsequently located in the pore.[4c,5] The most prevalent strains of influenza A have become resistant to common treatment methods, prompting additional interest in understanding the structure and function of M2, which could lead to the possibility of designing alternative small molecule inhibitors with which to treat this disease.[1,4a,6] The structure–function relationships of M2 have been studied by a variety of techniques, including X-ray diffraction,[3,6g,7] fluorescence imaging,[8] and both solution and magic angle spinning (MAS) NMR spectroscopies.[5a,b,6a,b,9]

A detailed understanding of the mechanism of proton conduction would form a foundation for an understanding of inhibition and resistant mutation. Historically, two models have been proposed to be responsible for proton conduction in M2, a water-wire or Grotthuss model and a shuttle model (transporter model), which may or may not involve a hydrogen-bonded dimer as an intermediate that could be integral to its function.[1,6c,d] In the water-wire model, as multiple protons enter the channel, electrostatic repulsion results in the expansion of the channel's diameter, allowing for protons to traverse the channel directly from one water molecule to another. The water-wire model would likely involve global

Received: May 6, 2014
Revised: September 2, 2014
Published: September 3, 2014

   dx.doi.org/10.1021/bi5005393 | *Biochemistry* 2014, 53, 5987–5994

changes to the protein structure upon protonation in order to facilitate proton transfer. In contrast, the shuttle model proceeds through several steps, beginning with protons entering the channel and binding to His 37, followed by His 37 ring motion,[4c,6b] which moves the proton from one side of the channel to the other, and last a deprotonation step that releases the proton on the other side of the channel. It has also been hypothesized that a hydrogen-bonded dimer (a state in which one proton is shared between adjacent His 37 residues) forms following initial protonation, based on previous measurements of His 37 in a transmembrane construct of M2. The shuttle model predicts that the proton conduction rate is a composite of both the degree of His 37 protonation and His 37 ring motion.[6b,c,10] In contrast, if the protein were switched open to form a water wire, then diffusion-limited conductance would be expected. Unlike the water-wire model, the shuttle model does not require global changes to the protein structure, although they may still occur.

Recent X-ray crystallography results from crystals of the transmembrane portion of M2 ($M2_{TM}$) formed at various pH's found differences in global protein structure, opening the possibility that changes in protein structures may occur during proton conduction and that the proton conduction model could be a combination of the water-wire and shuttle models. Unfortunately, there is limited information available to determine the exact mechanism of conduction, stemming from an absence of structural characterization of M2 at low pH, particularly when reconstituted in lipids.

The first study examining the protonation state of His 37 as a function of pH employing MAS NMR was performed by Cross et al. on $M2_{TM}$.[6d] By calculating the ratio of [His]/[HisH$^+$] from the ^{15}N MAS NMR spectrum as a function of pH, the authors generated a titration curve[11] for His 37, which yielded four pK_a's: 8.2, 8.2, 6.3, and <5.[6d] The degenerate pK_a of 8.2 was attributed to cooperative protonation as two protons entered the $M2_{TM}$ channel simultaneously, an unexpected result given the low dielectric environment of the transmembrane region and the fact that the pK_a of unperturbed histidine in aqueous solution is 6.2.[11,12] Hong et al. have also studied multiple aspects of $M2_{TM}$ by MAS NMR spectroscopy,[6a−c,10] including a detailed examination of the [His]/[HisH$^+$] of His 37 as a function of pH, which yielded four distinct pK_a's: 7.6 ± 0.1, 6.8 ± 0.1, 4.9 ± 0.3, and 4.2 ± 0.6.[6c] Hong et al. attributed the discrepancies between these two results to different fitting methods and to differences in the lipids used for reconstituting of the protein, which may impact protein structure or plasticity.[6c] They also measured the protonation/deprotonation rates of histidine, yielding an upper bound to the proton conduction rate for a shuttle mechanism, which was found to be within an order of magnitude of the measured conduction rate. The shuttle mechanism is therefore consistent with measured His 37 ring reorientation.[11,18,20]

While significant attention has been dedicated to understanding the model of proton conduction in constructs containing only the transmembrane portion of M2 ($M2_{TM}$), which consists of the residues 22−46, little attention has been devoted to longer constructs, many of which are fully functional and therefore possess characteristics closer to those of $M2_{WT}$ than of $M2_{TM}$ with respect to proton conduction and sensitivity to rimantadine.[13,14] One such functional construct is $M2_{18-60}$, which is composed of an unstructured N-terminus (18−23), a TM segment (25−46), and an amphipathic helix (51−59) at the C-terminus. The amphipathic helix forms a tetrameric domain separate from the TM tetramer with a head-to-tail assembly and a right handed packing mode in NMR structures and is known to stabilize tetramer formation.[1,6f,13b,15] Importantly, it has been demonstrated that constructs which possess the amphipathic helix display conductance[13a] and sensitivity to rimantadine[13b] similar to that of full-length M2. Therefore, we chose to study the pH behavior of $M2_{18-60}$.

Conduction properties and high-pH structural characteristics of $M2_{18-60}$ have been reported and are briefly described below. Pielak and Chou recently measured the proton conduction rates of $M2_{18-60}$ in liposomes as a function of pH, with the rate of proton conduction found to be inversely proportional to the pH of the solution with two pseudosaturation regions, one between pH 7.5 and 5.5 and another at pH < 4.[6f] Our group has recently examined the structure of $M2_{18-60}$ using MAS NMR spectroscopy[16] and observed doubling of many of the cross peaks in the spectra of $M2_{18-60}$ constructs of both WT and S31N, consistent with a C_2 symmetric quaternary structure of $M2_{18-60}$. In particular, in lipid bilayers, $M2_{18-60}$ adopts a dimer-of-dimers structure instead of a fully symmetric tetramer, which would have C_4 symmetry.[17] Recently, the dimer-of-dimers structure was also reported for the closely related $M2_{22-62}$ construct.[6e,18] Recently, a study examining an E3−M2 fusion protein via FRET in live cells indicated that the E3−M2 dimer forms at high pH's, that at low pH's tetramers are formed, and that conduction is possible with both dimers and tetramers. We note that these studies are conducted with a protein to lipid ratio of ∼1:1000, whereas MAS NMR studies need to be conducted with much lower lipid concentrations in order for a signal to be observed in a reasonable period of time.

Since $M2_{18-60}$ is known to fully reproduce the conduction and inhibition characteristics of the full-length protein,[13] as described above, and the structure of the construct is known to be different from that of $M2_{TM}$ for which His 37 pK_a's have been measured, we sought to understand the mechanism of proton gating by examining ^{15}N MAS NMR of $M2_{18-60}$ and to probe for any changes in structure as a function of pH with ^{13}C−^{13}C and ^{13}C−^{15}N correlations. In our present study, we have examined the H57Y variant to ensure that only one His is present in the primary sequence and reverse-labeled Ile, Leu, Phe, and Tyr residues in an effort to provide additional spectral resolution. Following refolding, the protein was adjusted to the appropriate pH in glutamate-citrate-phosphate buffer as described below. A titration curve was generated from the ^{15}N spectra of His 37 within $M2_{18-60}$ and simulated and surprisingly yielded only two proton association constants, 7.63 and 4.52. The plot of fraction of His 37 protonated as a function of pH closely matched a similar plot with the proton conduction rate measured as a function of pH, indicating that proton conduction rates are proportional to the protonation state of His 37, supporting the shuttle model for proton conduction. Imidazole proton chemical shifts revealed no evidence for proton sharing among adjacent His 37 residues. Two-dimensional ^{13}C−^{13}C and ^{13}C−^{15}N correlation spectroscopy reveals that as pH is lowered the protein accesses more conformations and no distinct shift to an open state is discernible.

EXPERIMENTAL SECTION

Synthesis and Reconstitution of U-^{13}C,^{15}N [Natural Abundance-ILFY]$M2_{18-60}$. Preparation of $M2_{18-60}$ by overexpression in *Escherichia coli* has been described previously.[17,19]

dx.doi.org/10.1021/bi5005393 | *Biochemistry* 2014, 53, 5987−5994

Briefly, $M2_{18-60}$ was overexpressed in *E. coli* BL-21 DE3 as a fusion with trpLE with an N-terminal His9-tag. Protein synthesis was induced with an IPTG concentration of 150 μM at an OD_{600} of 0.75. For reverse labeling, 1 L of M9 culture was divided into two parts. A 700 mL portion was inoculated and grown to an OD_{600} of 0.7. Natural abundance amino acids ILFY (Sigma) were dissolved in the remaining 300 mL and added to the 700 mL portion, bringing the OD to ~0.5 prior to induction at OD_{600} of 0.75. The culture was induced for 14−18 h at 18 °C. The protein was purified on a Ni^{2+} affinity column and cleaved with 0.35 g of cyanogen bromide in 2.5 mL of 70% formic acid per liter of cell culture. Finally, pure protein was isolated on a C4 reverse-phase HPLC column.

M2 Bilayer Preparation. Pure peptide was dispersed in 1,2-diphytanoyl-*sn*-glycerol-3-phosphocholine (DPhPC) purchased from Avanti. Bilayer samples were prepared by detergent dialysis. Peptide and lipid were dissolved separately in ~33 mg per mL of octyl glucopyranoside (OG) detergent (Sigma) and then combined at a 1:1 (w/w) lipid to protein ratio. Detergent was removed by dialyzing against 2 L of buffer with two buffer changes per day using a 3.5 kDa cutoff. Dialysis buffer contained 40 mM phosphate, 30 mM glutamate, and 3 mM sodium azide at pH 7.8. After 5 days of dialysis, the sample was pelleted by centrifugation at 100 000*g*. The pellet was suspended in buffer composed of 20 mM citric acid, 20 mM sodium phosphate, 40 mM glutamic acid, and 3 mM sodium azide, and the pH was subsequently adjusted to 3.5, 4.5, 5.5, 6.5, 7.5, and 8.5 with saturated NaOH and incubated for at least 24 h. This buffer was chosen for its ability to buffer from pH 3−9. Following equilibration, the samples were centrifuged at 100 000*g* for 2 h at 4 °C and packed into 3.2 mm Varian rotors.

NMR. One-dimensional ^{15}N spectra were recorded on a 500 MHz (11.7 T) spectrometer courtesy of Dr. David J. Ruben, using a 3.2 mm HCN Varian MAS probe at $\omega_r/2\pi$ = 10.5 kHz and regulated to ±10 Hz using a Bruker spinning frequency controller. The temperature was controlled with VT gas regulated at −6, 25, and 37 °C. The spectra were acquired with 83 kHz TPPM decoupling and a CP contact time of 1.5 ms.

ZF-TEDOR NMR spectra were recorded at 700 MHz ^1H frequency using a home-built spectrometer courtesy of Dr. David J. Rubin and a triple channel Varian 3.2 mm HCN probe. ^{13}C and ^{15}N chemical shifts were referenced using the published shifts of adamantine relative to DSS for ^{13}C referencing and the IUPAC relative frequency ratios between DSS (^{13}C) and liquid ammonia (^{15}N). Spectra acquired at 700 MHz were at $\omega_r/2\pi$ = 12.5 kHz. 83 kHz TPPM ^1H decoupling was used in all experiments. All spectra were recorded with VT gas regulated at the indicated temperature approximately 1 in. from the stator. Z-filtered transferred echo double resonance (ZF-TEDOR)[20] was acquired using 1.4 ms mixing with 50 kHz ^{13}C and ^{15}N π-pulses. The temperature under experimental conditions was measured to be 7 °C higher than the regulated VT cooling gas using the chemical shift of KBr according to the method reported by Thurber and Tycko.[21] ^1H detected spectra were recorded at $\omega_{0I}/2\pi$ = 750 MHz using a home-built spectrometer courtesy of Dr. David J. Rubin and a 1.3 mm HCN Bruker probe (Bruker Biospin, Billerica, MA) at $\omega_r/2\pi$ = 60 kHz. Fifteen kilohertz TPPM proton decoupling was used in all experiments. The pulse sequence used to record $^1H-^{15}N$ spectra utilizes a polarization transferred from ^1H to ^{15}N by cross-polarization (CP), which then evolves on ^{15}N for a time t_1 with 15 kHz of ^1H decoupling.[22] The ^{15}N signal is then stored along z, and the ^1H signal is saturated to minimize the signal from protons not bonded to ^{15}N. A second CP transfers signal from ^{15}N to ^1H, which is then detected. The CP contact time was 1.5 ms for the transfer from ^1H to ^{15}N, and contact times of 0.2 and 0.5 ms were used for the transfer from ^{15}N to ^1H in separate experiments. Spectra recorded at 700 and 750 MHz were processed, displayed, and assigned using the NMRPipe software package.[23]

RESULTS AND DISCUSSION

One-dimensional ^{15}N MAS NMR spectra of His 37 in $M2_{18-60}$ are shown at 25 °C and pH values indicated in Figure 1, with

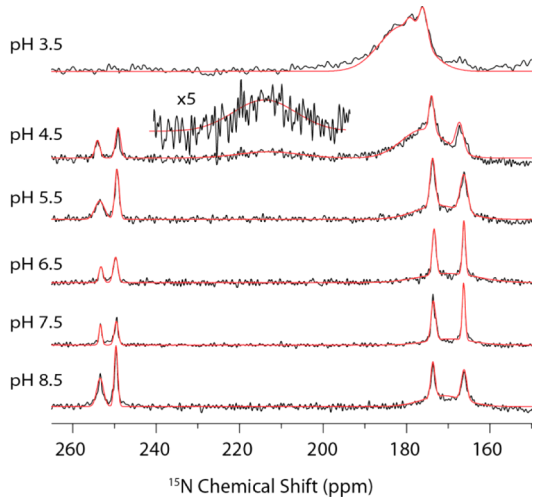

Figure 1. One-dimensional CP ^{15}N MAS NMR spectra of $M2_{18-60}$ H57Y ILFY at 500 MHz ^1H frequency and 25 °C ($\omega_r/2\pi$ = 10.5 kHz, CP contact time 1.5 ms, 83 kHz TPPM decoupling, and 75 000 transients per spectrum). Gaussian fits of the spectra are shown in red.

the corresponding spectra at −6 and 37 °C shown in Figure S1. We initially suspected, and later confirmed, that protonation of His 37 does not occur at pH 8.5, with the spectrum displaying four peaks at 166, 173, 249, and 253 ppm. The 166 and 173 ppm signals are attributed to protonated ^{15}N's, and the 249 and 253 ppm, due to unprotonated ^{15}N's.[11] Both sets of peaks correspond to the τ tautomer of His, as observed previously for the $M2_{18-60}$ construct.[16,17,19] The peak doubling is a result of the dimer-of-dimer structure reported previously[17] and was further confirmed by our ZF-TEDOR results that are illustrated extensively in Figures 2 and S3. It is unclear what drives the dimer-of-dimers formation in this construct; however, we note that it appears to be maintained throughout the titration presented herein and that some peak doubling was observed in a similar construct, $M2_{22-62}$.[18] The chemical shift of the four resonances do not shift substantially as the pH is decreased (Figure 1); however, the unprotonated signal intensities decrease, the two protonated signals increase, and a broad feature concomitantly appears centered at 175−180 ppm. The signal at 175−180 is found to be strongly temperature-dependent, as this feature is both broader and more pronounced as the temperature increases. On the basis of the chemical shift, this broad line is assigned to protonated ^{15}N's from an imidazolium ion in intermediate exchange between protonated and deprotonated states (Figure 3). Recent evidence points to water as the important hydrogen-bonding partner for imidazolium in $M2_{TM}$.[6c,12] The changes at pH 4.5

dx.doi.org/10.1021/bi5005393 | *Biochemistry* 2014, 53, 5987−5994

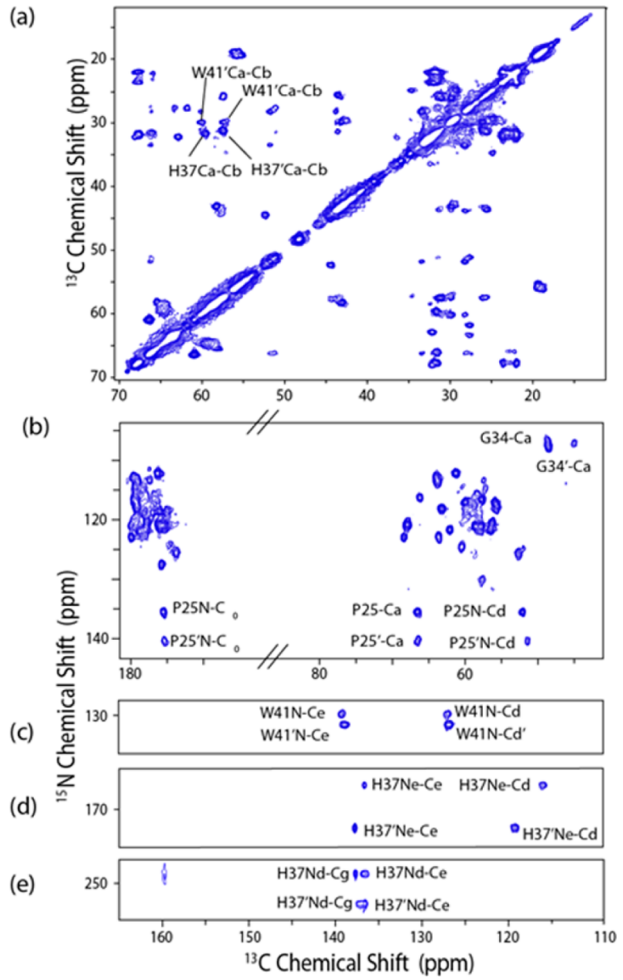

Figure 2. (a) Two-dimensional $^{13}C-^{13}C$ 20 ms PDSD of $M2_{18-60}$ H57Y ILFY (CP contact time 1.5 ms and 83 kHz TPPM decoupling) and (b) 2D $^{13}C-^{15}N$ 3.2 ms ZF-TEDOR of $M2_{18-60}$ H57Y ILFY both acquired at $\omega_r/2\pi$ = 12.5 kHz 700 MHz ^{1}H frequency, pH 7.5, and −6 °C. (c–e) Strips showing aromatic regions of the ZF-TEDOR. This data shows peak doubling indicative of dimer of dimer structure, even after protonation has partially occurred.

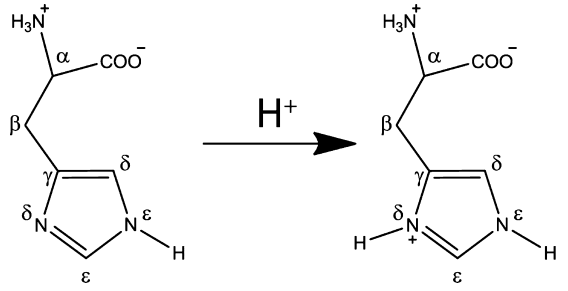

Figure 3. Schematic showing protonation of ε nitrogen in the neutral state. Protonation taking place as the pH is lowered occurs on the δ^1 nitrogen selectively.

are more immediately apparent, with a second broad signal present at 25 and 37 °C centered at 213 ppm, which corresponds to the average chemical shift of the protonated (~170 ppm) and unprotonated nitrogens (~250 ppm) and is attributed to rapid protonation and deprotonation between either ^{15}N's on adjacent His rings or between His and water within the channel.[6c] The 50% occupancy of the proton suggests a shared proton between two histidines, either directly or mediated by other hydrogen-bonding partners, such as water within the channel.[6c]

Since His has two N's, there are two possible tautomers in the neutral state, with the so-called π tautomer present when the δ-nitrogen is protonated and the τ tautomer present when the ε^2-^{15}N is protonated,[11] which is another detailed piece of information in the proton conduction model. Although tautomerization occurs rapidly in the solution state, it has been established that, in the solid state, tautomerization is slow, allowing both tautomers to be observed if they are present in the sample.[11] Both tautomers have been observed in previous studies of His 37 in $M2_{TM}$[6d] and in free histidine[11] and may also be present in $M2_{18-60}$. We therefore examined the ZF-TEDOR at pH 8.5 (Figure S3), where His 37 is in the neutral state, clearly showing that the protonated ^{15}N is exclusively the ε-^{15}N, schematically shown in Figure 3. This indicates that the τ tautomer is exclusively present initially, with no evidence for tautomerization observed by MAS NMR, and therefore the δ nitrogen is protonated as the pH is decreased.

The protonated ^{15}N's of histidine are known to have higher CP efficiencies compared with those of the unprotonated ^{15}N's due to their closer proximity to ^{1}H; therefore, the differences in CP efficiencies need to be accounted for to obtain genuine values of [HisH$^+$]/[His] as a function of pH.[6c,12] Equation 1[6c] was used to calculate the ratio of [HisH$^+$]/[His] as a function of pH.

$$\frac{[\mathrm{HisH}^+]}{[\mathrm{His}]} = \frac{(I_{\mathrm{NH}} - I_{\mathrm{N}}\kappa)/2}{I_{\mathrm{N}}\kappa} = \frac{((I_{\mathrm{NH}}/I_{\mathrm{N}})/\kappa) - 1}{2} \quad (1)$$

where I_N is the intensity of the unprotonated nitrogens, obtained by integration of the signals at 249 and 253 ppm, I_{NH} is the intensity of the protonated nitrogens likewise obtained by integration of the signals at 166 and 173 ppm, and κ is defined as the ratio of the integrated CP intensity of [HisH$^+$]/[His] in a neutral state.[6c,12] In our case, κ was found to be 1.83 at 37 °C, 1.56 at 25 °C, and 1.46 at −6 °C, with all values measured at pH 8.5. Although the value of κ should depend on the CP contact time and $\omega_r/2\pi$, we note that the values we observed are similar to those reported for $M2_{TM}$ at pH 8.5 (κ = 1.55)[6c] and crystalline histidine (κ = 1.464).[6c]

In the main text of this article, we have chosen to focus on the 25 °C data, as the temperature of the sample is ~7 °C higher than that of the VT gas once frictional heating and warming of the VT gas before reaching the probe are taken into account. [HisH$^+$]/[His] extracted from eq 1 is shown in Table 1 and displayed in Figure 4, along with simulations described below. The 1D ^{15}N MAS NMR spectra show similar features and trends compared to those of $M2_{TM}$ reported previously;[6c,d] however, the plot of [HisH$^+$]/[His] vs pH, extracted form eq 1, is different, with previous studies on $M2_{TM}$ showing a continual

Table 1. Ratio of Protonated Nitrogens and Unprotonated Nitrogens at 25 °C as a Function of pH

pH	I_{NH}/I_N	His$^+$/His
3.5	inf	50.1 ± 5.0
4.5	10.38	2.84 ± 0.40
5.5	4.69	1.01 ± 0.22
6.5	4.2	0.86 ± 0.20
7.5	2.91	0.439 ± 0.05
8.5	1.56	0.032 ± 0.01

dx.doi.org/10.1021/bi5005393 | Biochemistry 2014, 53, 5987−5994

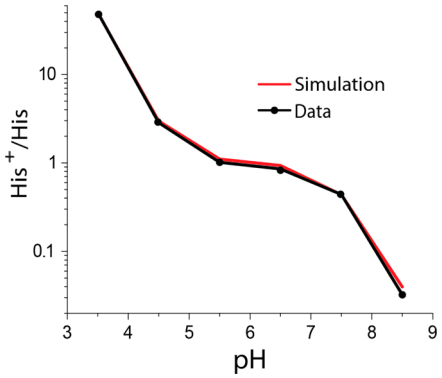

Figure 4. Ratio of $HisH^+$ to His as a function of pH at 25 °C. (Simulation of the experimental data is in red.)

increase in the protonation of the tetrad,[12,13] whereas our results show that within pH range 5.5−7.5 the level of protonation is relatively constant. $[HisH^+]/[His]$ is related to the maximum of four pK_a's according to eqs 2 and 3.[6c]

$$\frac{[HisH^+]}{[His]} = \frac{4[His_4H_4^{4+}] + 3[His_4H_3^{3+}] + 2[His_4H_2^{2+}] + [His_4H^+]}{[His_4H_3^{3+}] + 2[His_4H_2^{2+}] + 3[His_4H^+] + 4[His_4]} \quad (2)$$

$$\frac{[HisH^+]}{[His]} = \frac{4 + 3\frac{K_{a1}}{10^{-pH}} + 2\frac{K_{a1}K_{a2}}{10^{-2pH}} + 1\frac{K_{a1}K_{a2}K_{a3}}{10^{-3pH}}}{1\frac{K_{a1}}{10^{-pH}} + 2\frac{K_{a1}K_{a2}}{10^{-2pH}} + 3\frac{K_{a1}K_{a2}K_{a3}}{10^{-3pH}} + 4\frac{K_{a1}K_{a2}K_{a3}K_{a4}}{10^{-2pH}}} \quad (3)$$

The data points in Table 1 were fit with eq 3 using a home-written MATLAB program by searching a reduced chi-squared grid for the best fit of the data with random noise incorporated in a Monte Carlo manner, with the latter used to generate the error bars for the proton disassociation constants. Surprisingly, only two distinct proton disassociation constants were found, pK_{a1} = 7.63 ± 0.15 and pK_{a2} = 4.52 ± 0.15, despite the model allowing for a maximum of four pK_a's. We emphasize that our fitting of this data enables a maximum of four pK_a's and that it is possible that two distinct pK_a's exist and are close to one another but are not distinguishable from one another given the error of our measurements and simulations. Degeneracy of proton dissociation constants has been observed previously[6d] and was attributed to cooperativity in the protonation of the tetrameric channel, with the first protonation step making the second protonation more favorable, resulting in two protons entering the channel simultaneously. However, a second possibility should also be considered, namely, shielding of the interaction between the two charged side chains, where the two protons entering the channel have a negligible impact on each other's trajectory. Because the $M2_{18-60}$ tetrameric channel has C_2 symmetry, it is possible that each dimer within the larger tetramer could be protonated independently, which would manifest itself through similar pK_a's. Unfortunately, we were unable to distinguish between these two possibilities, but we note that noncooperativity appears to be a plausible option given the symmetry of the channel along with the absence of observed proton sharing, and it should be seriously considered alongside cooperative proton transfer. The pK_a's found are significantly different from the pK_a of native histidine[6d] and could be due to several possible explanations. The first pK_a (7.63 ± 0.15) is shifted up relative to that of free histidine and has previously been attributed in part to the presence of a cation−π interaction between His 37 and Typ 41, which stabilizes the charges within the channel and has been observed by resonance Raman spectroscopy.[24] Another possible explanation may be due to the proton being shared among more than one histidine within the channel, either directly through a low barrier hydrogen bond (LBHB)[4c,6d] or through a water molecule as an intermediate to transfer the proton.[13a,25] We sought to probe whether either of these possibilities is present in our system by recording the ^{1}H chemical shifts of His 37 in a ^{1}H-detected spectrum at high spinning frequency, $\omega_r/2\pi$ = 60 kHz. Figure 5 shows a ^{1}H−^{15}N correlation

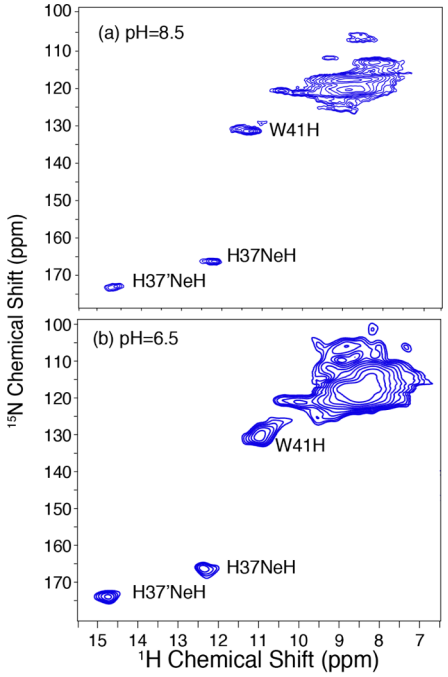

Figure 5. ^{1}H detected ^{1}H−^{15}N MAS correlation spectra at (a) pH 8.5 and (b) pH 6.5 of $M2_{18-60}$ H57Y ILFY (CP contact time 1 = 1.5 ms, CP contact time 2 = 0.2 ms. $\omega_{0I}/2\pi$ = 750 MHz, $\omega_r/2\pi$ = 60 kHz, 15 kHz TPPM decoupling, T = 30 °C).

experiment recorded at 750 MHz and 60 kHz, as described in the Experimental Section, at pH 8.5 and 6.5. These two pH values were chosen because the channel should possess neutral charge at pH 8.5 and should be predominantly in the +2 state at pH 6.5. Unfortunately, due to broadening at lower pH's, we were unable to obtain spectra under the acidic conditions necessary (pH 3.5) to observe the fully protonated state. ^{15}N signals corresponding to His 37 are clearly observed at both pHs, with cross peaks at 166 ppm/12.1 ppm and 173 ppm/14.5 ppm in the ^{15}N/^{1}H dimensions at pH 8.5 and with only a small shift in the proton dimension observed with cross peaks observed at 166 ppm/12.4 ppm and 173 ppm/14.8 ppm at pH 6.5. The small change in the proton chemical shift likely indicates that the uncharged and +2 charged states have similar hydrogen-bonding characteristics. We anticipate that a LBHB would not be present in the neutral state at pH 8.5, as the LBHB between adjacent His 37 is thought to exist in the protonated state of the His 37 tetramer. If a LBHB were present, then we would anticipate that the proton chemical shift would move downfield as the tetrad is protonated. Therefore, we conclude that although the chemical shifts are downfield we

dx.doi.org/10.1021/bi5005393 | Biochemistry 2014, 53, 5987−5994

do not believe this is indicative of a LBHB, as we anticipate a measurable change in the ^{1}H chemical shift in His 37 from pH 8.5 to 6.5.[26] As will be discussed below, the lowest temperature that we are able to achieve at this spinning frequency is ~30 °C and therefore we cannot rule out the possibility that a LBHB could be present at lower temperatures; however, we note that the spectra presented herein are close to physiological temperature and would be the most relevant set of conditions to study the proton mechanism. Another possibility to account for the proton sharing of His 37 is that the proton is hydrogen-bonded to an adjacent water molecule within the tetrameric channel. Hong et al. recently measured the ^{1}H−^{15}N correlation in $M2_{TM}$ using a HETCOR experiment, which showed that protonated His 37 is hydrogen-bonded to a water molecule within the channel.[25] This study also showed two cross peaks at 160 ppm/8 ppm and another at 170 ppm/10 ppm, with the proton chemical shift found to vary with pH. When the sample was frozen, they observed a cross peak between His 37 and water, indicating that the hydrogen-bonding partner is water; however, this feature was absent at elevated temperatures. The proton chemical shifts observed for $M2_{18-60}$ are shifted downfield relative to those reported for $M2_{TM}$, which is likely indicative of structural differences between $M2_{TM}$ and $M2_{18-60}$. We are unable to observe any cross peaks with water, as we estimate that the lowest temperature achievable at $\omega_r/2\pi$ = 60 kHz is ~30 °C.

While the first pK_a at 25 °C is shifted up to 7.63 ± 0.15, the second pK_a (4.52 ± 0.15) is shifted down from that of histidine as a result of electrostatic repulsion from placing the third and fourth protons inside the channel. It was recently proposed that cation−π interactions between His 37 and Trp 41 may be more pronounced at low pH and may help to offset the electrostatic repulsion in the fully protonated channel.[24]

Dissociation constants extracted from the spectra acquired at −6 and 37 °C were similar to those from 25 °C, with pK_a's of 7.42 ± 0.15 and 4.22 ± 0.15 at −6 °C and 7.55 ± 0.15 and 4.80 ± 0.15 at 37 °C. The initial protonation step seems to be relatively temperature-independent, as the pK_a's extracted are very similar and within the error of the measurement; however, the second protonation step shows a dependence on temperature, which indicates that the channel becomes increasingly easier to fully protonate at elevated temperatures. The second protonation step fully protonates the channel, and electrostatic repulsion is more likely to be a substantial factor in protonation compared to the initial protonation step. At elevated temperatures, His 37 should be more mobile, increasing the average distance between the charges, whereas at lower temperatures, the protein is expected to be less likely to access favorable geometries for the fully protonated state. We speculate that this is due to increased mobility of the protein, which would allow the histidines to move away from one another, partially offsetting the electrostatic repulsion. We also considered that the pK_a's of the buffer components may be temperature-dependent and therefore alter the pH of the buffer at various temperatures, with the temperature dependence of His 37's pK_a's being a result of temperature-dependent changes in the pH of the buffer. The pK_a's of citrate and glutamic acid should be most relevant to the pH between 4 and 6, which decrease as temperature is increased, by about 0.04 units over the relevant temperature range.[27] This should result in a decrease in pH as temperature is increased and should have an impact on the fitted proton dissociation constants, but it should do so only modestly and therefore it does not account for the entirety of the temperature-dependent pK_a's.

The plot of [HisH$^+$]/[His] vs pH (Figure 4) is qualitatively similar to the analogous plot of proton conduction reported previously using the $M2_{18-60}$ construct including the pseudosaturation region over a similar pH range[6f] and implies that the rate of proton conduction is directly proportional to [HisH$^+$]/[His]. The pK_a's extracted from our data indicates that at pH < 3.5 $M2_{18-60}$ is >95% protonated. If the shuttle model is responsible for proton conduction, then the rate of proton conduction should be dictated by both the rate of small angle rotations of His 37's ring and whether a proton is bound to His 37. Thus, at pH < 3.5, the protonation of the histidine has saturated, leaving the ring motion of histidine to limit the proton conduction rate and resulting in a maximum rate that explains the second saturation region observed in the proton conduction data.[6f]

Lastly, we sought to determine if any global structural changes were observed within the protein as a function of pH; therefore, we acquired one-bond ^{13}C−^{13}C and ^{13}C−^{15}N correlations from PDSD and ZF-TEDOR experiments, shown in Figures 2, S2, and S3. We anticipate that if other stable structures are present at various pH's, then we would observe chemical shift changes. However, as the pH was decreased, no changes in the chemical shifts of the cross peaks were observed; instead, we found a progressive broadening and eventual disappearance of cross peaks at the lowest pHs, which limited our ability to probe the structure of the protein in the high-conductance +3 state. The broadening suggests that the protein is able to access multiple conformations at low pH, and the disappearance of peaks indicates that the sample is more dynamic. This is consistent with the earlier observation on the same protein construct using solution NMR in which decreasing the pH from 7.5 to 6.0 caused nearly complete broadening of resonances of the transmembrane helices.[15a] We attempted to record INEPT spectra at all pH's to determine if any of the protein was highly mobile, but no INEPT signal was observed (data not shown). Thus, MAS NMR spectra do not indicate global changes in protein structure as a function of pH, which was observed by X-ray crystallography.

■ CONCLUSIONS

MAS NMR was used to measure the pH-dependent protonation of $M2_{18-60}$ in the dimer-of-dimers structure. The level of protonation observed in the spectra correlates with previously measured proton conduction rates, supporting the shuttle model of proton transfer. The second protonation step is found to be temperature-dependent and is likely due to electrostatic repulsion from the four protons in the fully protonated state. We also show that $M2_{18-60}$ accesses more conformations in acidic solutions and that a stable open-state structure is not triggered by protonation. The ^{1}H chemical shifts of H37 side chains showed no evidence for a LBHB among His 37 residues. Taken together, the data suggest that the first doubly degenerate pK_a is shifted up due to cation−π interactions, whereas the second doubly degenerate pK_a is shifted down due to electrostatic interactions. The third and fourth protonation events occur more frequently at the low endosomal pH, leading to conduction via the shuttle mechanism.

dx.doi.org/10.1021/bi5005393 | Biochemistry 2014, 53, 5987−5994

■ ASSOCIATED CONTENT

Supporting Information

Ratio of protonated nitrogens to unprotonated nitrogen as a function of pH and temperature, ^{15}N MAS NMR spectra of $M2_{18-60}$ H57Y ILFY, 2D ^{13}C−^{13}C 20 ms PDSD spectra of $M2_{18-60}$, and 2D ^{13}C−^{13}C 3.2 ms ZF-TEDOR spectra of $M2_{18-60}$. This material is available free of charge via the Internet at http://pubs.acs.org.

■ AUTHOR INFORMATION

Corresponding Author

*E-mail: rgg@mit.edu.

Author Contributions

M.T.C. and L.B.A. prepared the M2 samples, recorded the MAS NMR spectra, and fit and analyzed the data. M.T.C., L.B.A., J.J.C., and R.G.G. wrote the manuscript.

Funding

This work was supported by the National Institute of Biomedical Imaging and Bioengineering of the National Institute of Health under grant nos. EB001960, EB002026, and GM094648.

Notes

The authors declare no competing financial interest.

■ ACKNOWLEDGMENTS

The authors than Dr. Marcel Reese for useful discussions.

■ REFERENCES

(1) Pielak, R. M., and Chou, J. J. (2011) Influenza M2 proton channels. *Biochim. Biophys. Acta, Biomembr. 1808*, 522−529.

(2) (a) Lin, T. I., and Schroeder, C. (2001) Definitive assignment of proton selectivity and attoampere unitary current to the M2 ion channel protein of influenza A virus. *J. Virol. 75*, 3647−56. (b) Mould, J. A., Drury, J. E., Frings, S. M., Kaupp, U. B., Pekosz, A., Lamb, R. A., and Pinto, L. H. (2000) Permeation and activation of the M2 ion channel of influenza A virus. *J. Biol. Chem. 275*, 31038−31050.

(3) Rossman, J. S., and Lamb, R. A. (2011) Influenza virus assembly and budding. *Virology 411*, 229−236.

(4) (a) Wang, C., Lamb, R. A., and Pinto, L. H. (1995) Activation of the M2 ion channel of influenza virus: a role for the transmembrane domain histidine residue. *Biophys. J. 69*, 1363−1371. (b) Tang, Y., Zaitseva, F., Lamb, R. A., and Pinto, L. H. (2002) The gate of the influenza virus M2 proton channel is formed by a single tryptophan residue. *J. Biol. Chem. 277*, 39880−39886. (c) Sharma, M., Yi, M. G., Dong, H., Qin, H. J., Peterson, E., Busath, D. D., Zhou, H. X., and Cross, T. A. (2010) Insight into the mechanism of the influenza A proton channel from a structure in a lipid bilayer. *Science 330*, 509−512.

(5) (a) Cady, S. D., Schmidt-Rohr, K., Wang, J., Soto, C. S., DeGrado, W. F., and Hong, M. (2010) Structure of the amantadine binding site of influenza M2 proton channels in lipid bilayers. *Nature 463*, 689−692. (b) Cady, S. D., Wang, J., Wu, Y., DeGrado, W. F., and Hong, M. (2011) Specific binding of adamantane drugs and direction of their polar amines in the pore of the influenza M2 transmembrane domain in lipid bilayers and dodecylphosphocholine micelles determined by NMR spectroscopy. *J. Am. Chem. Soc. 133*, 4274−4284. (c) Pielak, R. M., Oxenoid, K., and Chou, J. J. (2011) Structural investigation of rimantadine inhibition of the AM2−BM2 chimera channel of influenza viruses. *Structure 19*, 1655−1663. (d) Jing, X. H., Ma, C. L., Ohigashi, Y., Oliveira, F. A., Jardetzky, T. S., Pinto, L. H., and Lamb, R. A. (2008) Functional studies indicate amantadine binds to the pore of the influenza A virus M2 proton-selective ion channel. *Proc. Natl. Acad. Sci. U.S.A. 105*, 10967−10972. (e) Stouffer, A. L., Acharya, R., Salom, D., Levine, A. S., Di Costanzo, L., Soto, C. S., Tereshko, V., Nanda, V., Stayrook, S., and DeGrado, W. F. (2008) Structural basis for the function and inhibition of an influenza virus proton channel. *Nature 451*, 596−599. (f) Yi, M., Cross, T. A., and Zhou, H. X. (2008) A secondary gate as a mechanism for inhibition of the M2 proton channel by amantadine. *J. Phys. Chem. B 112*, 7977−7979.

(6) (a) Hu, F., Luo, W., Cady, S. D., and Hong, M. (2011) Conformational plasticity of the influenza A M2 transmembrane helix in lipid bilayers under varying pH, drug binding, and membrane thickness. *Biochim. Biophys. Acta 1808*, 415−423. (b) Hu, F., Luo, W., and Hong, M. (2010) Mechanisms of proton conduction and gating in influenza M2 proton channels from solid-state NMR. *Science 330*, 505−508. (c) Hu, F., Schmidt-Rohr, K., and Hong, M. (2012) NMR detection of pH-dependent histidine-water proton exchange reveals the conduction mechanism of a transmembrane proton channel. *J. Am. Chem. Soc. 134*, 3703−3713. (d) Hu, J., Fu, R., Nishimura, K., Zhang, L., Zhou, H. X., Busath, D. D., Vijayvergiya, V., and Cross, T. A. (2006) Histidines, heart of the hydrogen ion channel from influenza A virus: toward an understanding of conductance and proton selectivity. *Proc. Natl. Acad. Sci. U.S.A. 103*, 6865−6870. (e) Miao, Y. M., Qin, H. J., Fu, R. Q., Sharma, M., Can, T. V., Hung, I., Luca, S., Gor'kov, P. L., Brey, W. W., and Cross, T. A. (2012) M2 proton channel structural validation from full-length protein samples in synthetic bilayers and *E. coli* membranes. *Angew. Chem., Int. Ed. 51*, 8383−8386. (f) Pielak, R. M., and Chou, J. J. (2010) Kinetic analysis of the M2 proton conduction of the influenza virus. *J. Am. Chem. Soc. 132*, 17695−17697. (g) Wang, J., Wu, Y. B., Ma, C. L., Fiorin, G., Wang, J. Z., Pinto, L. H., Lamb, R. A., Klein, M. L., and DeGrado, W. F. (2013) Structure and inhibition of the drug-resistant S31N mutant of the M2 ion channel of influenza A virus. *Proc. Natl. Acad. Sci. U.S.A. 110*, 1315−1320.

(7) (a) Duque, M. D., Ma, C. L., Torres, E., Wang, J., Naesens, L., Juarez-Jimenez, J., Camps, P., Luque, F. J., DeGrado, W. F., Lamb, R. A., Pinto, L. H., and Vazquez, S. (2011) Exploring the size limit of templates for inhibitors of the M2 ion channel of influenza A virus. *J. Med. Chem. 54*, 2646−2657. (b) Polishchuk, A. L., Lear, J. D., Ma, C. L., Lamb, R. A., Pinto, L. H., and DeGrado, W. F. (2010) A pH-dependent conformational ensemble mediates proton transport through the influenza A/M2 protein. *Biochemistry 49*, 10061−10071.

(8) Lakadamyali, M., Rust, M. J., Babcock, H. P., and Zhuang, X. (2003) Visualizing infection of individual influenza viruses. *Proc. Natl. Acad. Sci. U.S.A. 100*, 9280−9285.

(9) (a) Li, C., Qin, H., Gao, F. P., and Cross, T. A. (2007) Solid-state NMR characterization of conformational plasticity within the transmembrane domain of the influenza A M2 proton channel. *Biochim. Biophys. Acta 1768*, 3162−3170. (b) Luo, W., and Hong, M. (2010) Conformational changes of an ion channel detected through water-protein interactions using solid-state NMR spectroscopy. *J. Am. Chem. Soc. 132*, 2378−2384.

(10) Hong, M., Zhang, Y., and Hu, F. H. (2012) Membrane protein structure and dynamics from NMR spectroscopy. *Annu. Rev. Phys. Chem. 63*, 1−24.

(11) Munowitz, M., Bachovchin, W. W., Herzfeld, J., Dobson, C. M., and Griffin, R. G. (1982) Acid-base and tautomeric equilibria in the solid-state: ^{15}N NMR spectroscopy of histidine and imidazole. *J. Am. Chem. Soc. 104*, 1192−1196.

(12) McGlinchey, R. P., Shewmaker, F., Hu, K. N., McPhie, P., Tycko, R., and Wickner, R. B. (2011) Repeat domains of melanosome matrix protein Pmel17 orthologs form amyloid fibrils at the acidic melanosomal pH. *J. Biol. Chem. 286*, 8385−8393.

(13) (a) Tobler, K., Kelly, M. L., Pinto, L. H., and Lamb, R. A. (1999) Effect of cytoplasmic tail truncations on the activity of the M(2) ion channel of influenza A virus. *J. Virol. 73*, 9695−9701. (b) Pielak, R. M., Schnell, J. R., and Chou, J. J. (2009) Mechanism of drug inhibition and drug resistance of influenza A M2 channel. *Proc. Natl. Acad. Sci. U.S.A. 106*, 7379−7384.

(14) Cross, T. A., Sharma, M., Yi, M., Dong, H., Qin, H., Peterson, E., Busath, D. D., and Zhou, H. X. (2011) *The native M2 proton channel structure from influenza A*, European Biophysical Congress, Budapest, Hungary, August 23−27.

(15) (a) Schnell, J. R., and Chou, J. J. (2008) Structure and mechanism of the M2 proton channel of influenza A virus. *Nature 451*, 591−595. (b) Salom, D., Hill, B. R., Lear, J. D., and DeGrado, W. F. (2000) pH-dependent tetramerization and amantadine binding of the transmembrane helix of M2 from the influenza A virus. *Biochemistry 39*, 14160−14170.
(16) Andreas, L. B., Barnes, A. B., Corzilius, B. r., Chou, J. J., Miller, E. A., Caporini, M., Rosay, M., and Griffin, R. G. (2013) Dynamic nuclear polarization study of inhibitor binding to the $M2_{18-60}$ proton transporter from influenza A. *Biochemistry 52*, 2774−2782.
(17) Andreas, L. B., Eddy, M. T., Chou, J. J., and Griffin, R. G. (2012) Magic-angle-spinning NMR of the drug resistant S31N M2 proton transporter from influenza A. *J. Am. Chem. Soc. 134*, 7215−7218.
(18) Can, T. V., Sharma, M., Hung, I., Gor'kov, P. L., Brey, W. W., and Cross, T. A. (2012) Magic angle spinning and oriented sample solid-state NMR structural restraints combine for influenza A M2 protein functional insights. *J. Am. Chem. Soc. 134*, 9022−9025.
(19) Andreas, L. B., Eddy, M. T., Pielak, R. M., Chou, J., and Griffin, R. G. (2010) Magic angle spinning NMR investigation of influenza A $M2_{18-60}$: support for an allosteric mechanism of inhibition. *J. Am. Chem. Soc. 132*, 10958−10960.
(20) Jaroniec, C. P., Filip, C., and Griffin, R. G. (2002) 3D TEDOR NMR experiments for the simulaneous measurement of multiple carbon-nitrogen distances in uniformly ^{13}C,^{15}N labeled solids. *J. Am. Chem. Soc. 124*, 10728−10742.
(21) Thurber, K. R., and Tycko, R. (2009) Measurement of sample temperatures under magic-angle spinning from the chemical shift and spin-lattice relaxation rate of 79 Br in KBr powder. *J. Magn. Reson. 196*, 84−87.
(22) Zhou, D. H., and Rienstra, C. M. (2008) High-performance solvent suppression for proton detected solid-state NMR. *J. Magn. Reson. 192*, 167−172.
(23) Delaglio, F., Grzesiek, S., Vuister, G. W., Zhu, G., Pfeifer, J., and Bax, A. (1995) NMRPipe—a multidimensional spectral processing system based on Unix pipes. *J. Biomol. NMR 6*, 277−293.
(24) (a) Czabotar, P. E., Martin, S. R., and Hay, A. J. (2004) Studies of structural changes in the M2 proton channel of influenza A virus by tryptophan fluorescence. *Virus Res. 99*, 57−61. (b) Okada, A., Miura, T., and Takeuchi, H. (2001) Protonation of histidine and histidine−tryptophan interaction in the activation of the M2 ion channel from influenza A virus. *Biochemistry 40*, 6053−6060. (c) Williams, J. K., Zhang, Y., Schmidt-Rohr, K., and Hong, M. (2013) pH-dependent conformation, dynamics, and aromatic interaction of the gating tryptophan residue of the influenza M2 proton channel from solid-state NMR. *Biophys. J. 104*, 1698−1708.
(25) Hong, M., Fritzsching, K. J., and Williams, J. K. (2012) Hydrogen-bonding partner of the proton-conducting histidine in the influenza M2 proton channel revealed from ^{1}H chemical shifts. *J. Am. Chem. Soc. 134*, 14753−14755.
(26) (a) Zheng, L., Fishbein, K. W., Griffin, R. G., and Herzfeld, J. (1993) Two-dimensional solid-state proton NMR and proton exchange. *J. Am. Chem. Soc. 115*, 6254−6261. (b) Zheng, L., Fishbein, K. W., Griffin, R. G., and Herzfeld, J. (1993) Proton diffusion studied by solid-state 2D and 3D MAS ^{1}H NMR. *Biophys. J. 64*, A212.
(27) (a) Goldberg, R. N., Kishore, N., and Lennen, R. M. (2002) Thermodynamic quantities for the ionization reactions of buffers. *J. Phys. Chem. Ref. Data 31*, 231−370. (b) Nagai, H., Kuwabara, K., and Carta, G. (2008) Temperature dependence of the dissociation constants of several amino acids. *J. Chem. Eng. Data 53*, 619−627.